Reconstitution of the host holobiont acutely increases bone growth of the gnotobiotic rat

Czernik, PJ[1,3], Golonka, RM[1,2,3], Chakraborty, S[1,2,3], Yeoh, BS[1,2,3], Saha, P[1,2,3], Mell, B[1,2,3], Tian, Y[5], Patterson, AD[5], Joe, B[1,2,3], Vijay-Kumar, M[1,2,3*], Lecka-Czernik, B[1,3,4*]

[1]Microbiome Consortium, [2]Center for Hypertension and Precision Medicine and [3]Department of Physiology and Pharmacology, [4]Department of Orthopedic Surgery, University of Toledo College of Medicine and Life Sciences, Toledo, Ohio; [5]Department of Veterinary & Biomedical Sciences, The Pennsylvania State University, University Park, PA

*Corresponding authors:

Beata Lecka-Czernik, PhD
Department of Orthopaedic Surgery, Mail Stop 1008
College of Medicine and Life Sciences
University of Toledo
Toledo, Ohio 43614
Phone: 419-383-4140
Beata.Leckaczernik@utoledo.edu

Matam Vijay Kumar, PhD
Department of Physiology and Pharmacology, Mail Stop 1008
College of Medicine and Life Sciences
University of Toledo
Toledo, Ohio 43614
Phone: 419-383-4130
MatamVijay.Kumar@utoledo.edu

Abstract

The effect of microbiota on skeletal growth in adolescence has not been studied. Here, we present for the first time, an accelerated longitudinal and radial bone growth in response to short-term exposure of young germ-free rats to newly established gut microbiota. Seven-week-old germ-free male rats were colonized with microbiota through co-housing with conventional rats of the same sex and age. Changes in bone mass and structure were analyzed 10 days following the onset of colonization and revealed unprecedented acceleration of bone accrual, increased bone tissue mineral density, improved proliferation and hypertrophy of growth plate chondrocytes, and bone lengthening. The observed changes in bone status were paralleled with a dramatic increase in cecal concentration of short-chain fatty acids and increased hepatic *Igf-1* expression implicating an involvement of the somatotropic axis. Our studies demonstrate that gut microbiota can deliver powerful signals to the skeleton and accelerate bone expansion resembling adolescent growth spurt.

Introduction

Coined by Lynn Margulis in 1991, the term holobiont describes how macro-species, such as mammals, live in symbiosis with micro-species, whereby all individuals that participate in a particular symbiosis are bionts and the entire organism that is comprised of these bionts is a holobiont (Margulis & Fester, 1991; Simon et al., 2019). The human body is therefore a holobiont hosting an incredible number of microbial cells exceeding the number of cells in the entire human body (Sender et al., 2016). During evolution, these commensal microbes have colonized and co-evolved with the host as part of an internal ecosystem that orchestrates normal physiology. Any alteration in the composition of the micro-species, termed as microbial dysbiosis, is bound to affect normal physiology of the host.

In the last decade the concept of utilizing a reconstitution or correction to the gut microbiome as a therapeutic agent has been in various stages of development, none of them has received regulatory approval yet. Nonetheless, extensive studies in experimental animals on the level of basic research and ongoing clinical trials involving microbiota (Medicine, 2020) are very promising in delivering means of medical intervention to mitigate incurable conditions and augment existing therapies for treatment of recurring intestinal infections, bowel diseases, obesity, type 2 diabetes, osteoporosis and osteoarthritis (Davis, 2016; Gurung et al., 2020; Weingarden & Vaughn, 2017; Xu et al., 2017).

Contrasting effects of gut microbiota on bone formation in rats and mice have been reported. These disparities could result from the physiologic sensitivity of the gut microbiota-host relationship, where the experimental model, length of bacterial colonization, animal sex, strain, and age (Sjögren et al., 2012; Yan & Charles, 2017), and even housing environment and vendor

(Hernandez et al., 2016; Kang et al., 2015) variables can influence the gut microbiota-bone axis. A number of studies showed a positive effect of microbiota on bone in animal models of skeletal deficiencies and pathologies, as well as in humans with senile osteoporosis (Britton et al., 2014; Li et al., 2016; Park et al., 2017; Schepper et al., 2017; Xu et al., 2017). These studies have been aimed at finding novel remedies for bone-related ailments by utilizing bone-microbiota relationship as a target for intervention. However, the fundamental question of whether the holobiont derives signals from microbiota to facilitate host bone growth remains unanswered. Addressing this question will be important to exploit this synergy within the holobiont to bolster bone health of the host. Thus, in this study, we sought to examine the impact of acute exposure of the host to microbiota on bone growth using the experimental design of comparing bone mass and microarchitecture between gnotobiotic rats, which are depleted of microbiota and thereby represent the incomplete holobiont, and gnotobiotic rats reconstituted with microbiota which represent the complete holobiont. Altogether, this study unveils that the microbiota is imperative for skeletal homeostasis, where replenishing the micro-species rectifies bone growth that is stunted in microbiota ablation conditions.

Results

Reconstitution of the holobiont with microbiota increases bone mass of the host

To assess the immediate effect of gut microbiota on bone status we compared conventionalized germ-free rats (GFC) to their gnotobiotic or germ-free (GF) counterparts. Evaluation of cortical bone parameters at tibia midshaft and trabecular bone morphometry of proximal tibia were conducted using 3D images acquired by micro computed tomography (Fig. 1A and 1B). Cortical bone measurements revealed that within the short period of 10 days, GFC rats significantly gained bone mass. Total cross-sectional area (T.Ar), bone area (B.Ar), and cortical thickness

(Ct.Th) increased by 12.6%, 15.6%, and 11%, respectively (Fig. 1C-E). Marrow area (M.Ar) remained the same in both groups indicating that bone apposition in GFC rats occurred mainly on the periosteal surface (Supplementary Table 2). Body weight average for GFC rats was significantly increased by 27.3% (GF mean 205.7 g $\pm$ SD 30.2, GFC mean 261.8 g $\pm$ SD 13.3, p=0.002) suggesting that bone expansion may result from increased mechanical loading. However, while calculation of Pearson correlation coefficient (r) for cortical parameters versus body weight of GF animals showed that B.Ar (r=0.86), T.Ar (r=0.99), and Ct.Th (r=0.68) positively correlated with animal weights, in GFC animals T.Ar correlation was significantly lower (r=0.45) and B.Ar and Ct.Th correlated negatively with respective r values of -0.39 and -0.78. These data suggest that mechanical loading is not a major factor in driving cortical bone accrual. Instead, it may be associated with increased nutrition provided by gut microbiota fermentation of complex carbohydrates, but more importantly resulting from a molecular signaling along the gut-bone axis. It is important to stress that bone mass gain judged by an increase of mean cortical thickness in GFC rats was extensive considering the short time exposure to gut microbiota in GFC rats. Reported periosteal bone apposition rate in male rats of comparable age and body weight is on average 0.05 micron/hour (Stenstrom et al., 1977; Tam et al., 1978). Mean difference in cortical thickness between GF and GFC rats at the time of sacrifice was 47 micron, and gained over 10 days, giving an apparent apposition rate of 0.19 micron/hour. At the same time tissue mineral density (TMD) (Fig. 1F) in cortical bone was statistically increased in GFC rats but only by 2.1% which seemed to be less than expected for 4-fold increase in the apposition rate. Finally, calculations of bone moment of inertia at tibia midshaft showed that in GFC rats predicted bending strength perpendicular to the minimal (Imin) and maximal (Imax) axes of the bone cross sections were statistically increased, as well as

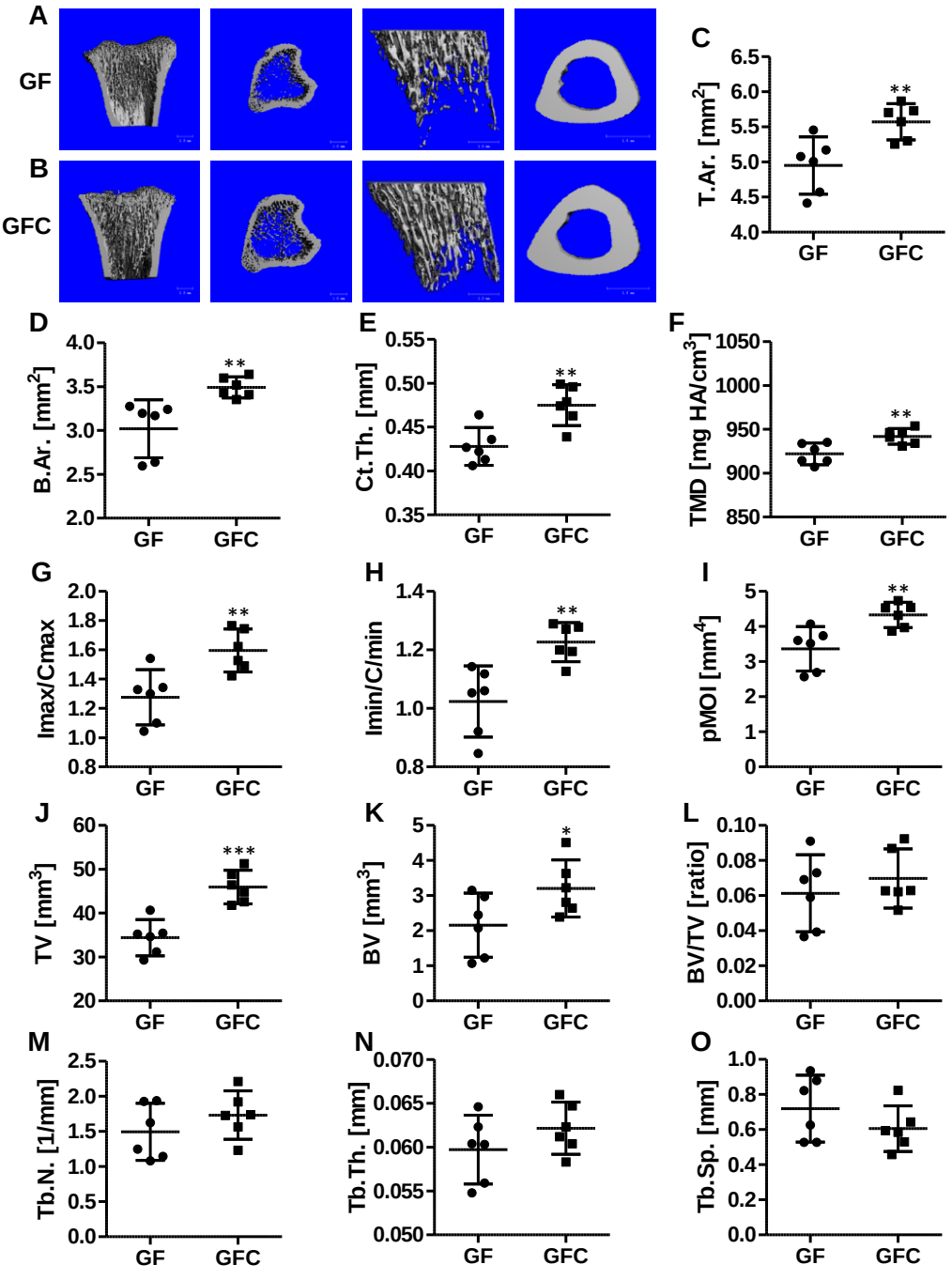

Figure 1. Acute effect of gut microbiota on bone mass and structure in germ-free conventionalized rats. A and B. mCT bone renderings of tibia of GF (A) and GFC (B) rats. From left to right: proximal tibia longitudinal sections, transverse sections 2 mm down from growth plate, trabecular bone compartment, and bone cross sections at tibia midshaft. C – F. Measurements of cortical bone at tibia midshaft. T.Ar – total area; B.Ar – bone area; Ct.Th – cortical thickness; TMD – tissue mineral density. G – I. Computed moment of inertia show respectively resistance to bending (Imax/Cmax, Imin/Cmin) and torsion (pMOI). J – O. Proximal tibia trabecular bone morphometry. TV – tissue volume; BV – bone volume, BV/TV – bone mass ratio; Tb.N – trabecular number; Tb.Th – trabecular thickness; Tb.Sp – trabecular spacing. *: $p<0.05$, **: $p<0.01$, ***: $p<0.001$

the torsional strength along the bone (Fig. 1G-I). Cumulatively, our findings imply that gut microbiota is capable of inducing an acute response resulting in bone mass increase and enhancement in bone mechanical properties. Measurements of trabecular bone in proximal tibia revealed statistical gains in total volume and bone volume with bone volume/total volume ratio remaining unchanged (Fig. 1J-L). This indicated overall bone expansion without formation of additional trabeculae. On the other hand, trabecular number and thickness were slightly increased and trabecular spacing was consequently decreased in GFC rats (Fig. 1M-O). While these differences albeit not statistically significant, nevertheless indicated the same trend of bone gain as observed in cortical bone. Assessment of trabecular bone in L4 vertebral body did not show significant differences in morphometric parameters except for the total bone size increase in GFC rats (Supplementary Table 3).

Periosteal bone apposition increases cortical bone mass

Micro CT measurements of cortical bone at tibia midshaft showed significant bone mass accumulation in GFC rats and implied that periosteal bone apposition was responsible for this increase. However, this analysis was conducted on a thin 0.5 mm tomographic segment of tibia. In order to validate this result on a broader scale and to get an insight into the nature of bone accumulation on a cellular level, we conducted histologic analysis of approximately 12 mm longitudinal sections of tibia diaphysis. Microscopic examinations of these specimens clearly demonstrated noticeable differences between GF and GFC rats in the distribution of circumferential lamellar bone. Measurements of areas occupied by lamellar bone on the periosteal surfaces showed an enlargement of this compartment by 5-fold with mean thickness increased over 2-fold in GFC versus GF rats (Fig. 2A-C). On the endosteal surfaces, area and mean thickness were quite the same in both animals (Fig. 2A and 2B). These results indicate that

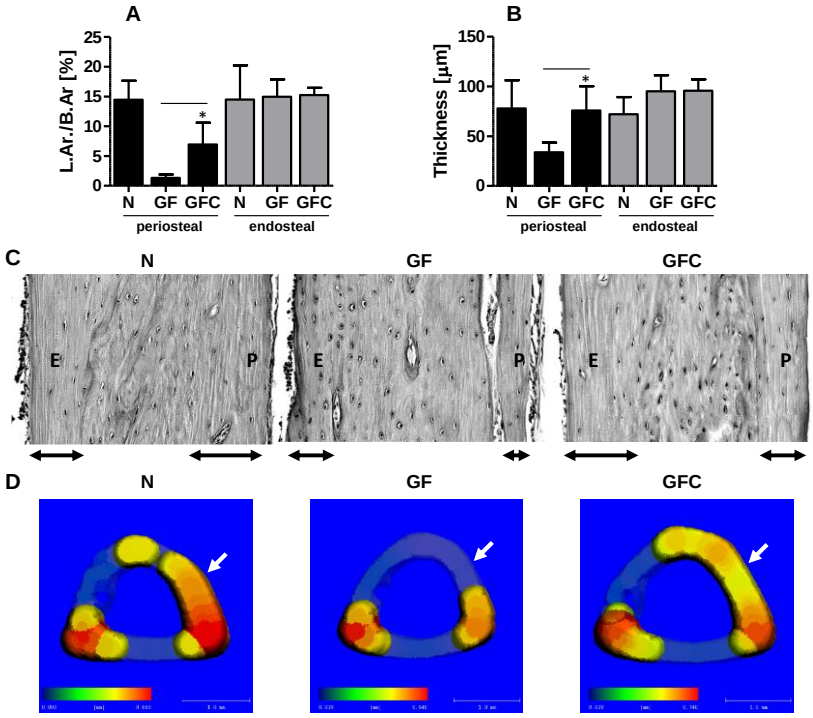

Figure 2. Circumferential lamellar bone apposition in tibia diaphysis of GF and GFC rats. A. Percent of periosteal bone (black bars) and endosteal bone (grey bars) occupied by lamellar bone in normal (N), GF and GFC rats. B. Mean thickness of the same bone regions. C. Images of representative histologic specimens of cortical bone used for measurements of N, GF, and GFC rats. Two-headed arrows indicate the extent of lamellar bone. P – periosteal bone; E – endosteal bone. D. Representative mCT renderings of tibia midshaft cross sections showing distribution of bone thickness in N, GF, and GFC rats over 0.44 mm thickness threshold. Blue color in scale bar indicate 0.0 mm thickness, red color indicates maximum thickness for given specimen. Transparent bone sections show thickness below 0.44 mm, white arrows point towards anteromedial bone surface. *: $p<0.05$

indeed accelerated periosteal bone apposition is likely responsible for increased cortical bone mass in GFC rats. Histologic specimens used for these measurements were cut longitudinally and parallel to anterior-posterior axis of tibia, therefore only anterior and posterior surfaces could be measured in these specimens. In order to assess the distribution of change in thickness around the tibia shaft we analyzed 4 tomographic slices spaced evenly along the length and location comparable to histologic specimens. Visualizations of local thicknesses were obtained in these slices using conventional sphere method of distance transformation available in our image analysis software package. Interestingly, the increase in bone thickness in GFC animals was

localized to the anteromedial section of the cortex and spanning approximately 1/3 of the bone circumference (Fig. 2D). This section of the tibia receives most of the strain (Gross et al., 2002). Assuming that GF and GFC animals experience a comparable bone adaptation to habitual mechanical loading the observed difference in local bone thickness suggests that microbiota accelerate osteogenesis around sites subjected to increased mechanical stimulation.

Microbiota stimulate growth plate enlargement, chondrocyte maturation and longitudinal bone growth

In the course of characterizing a skeletal response to the reconstitution of the holobiome, we measured differences in tibial length between GF and GFC rats and assessed morphology of the

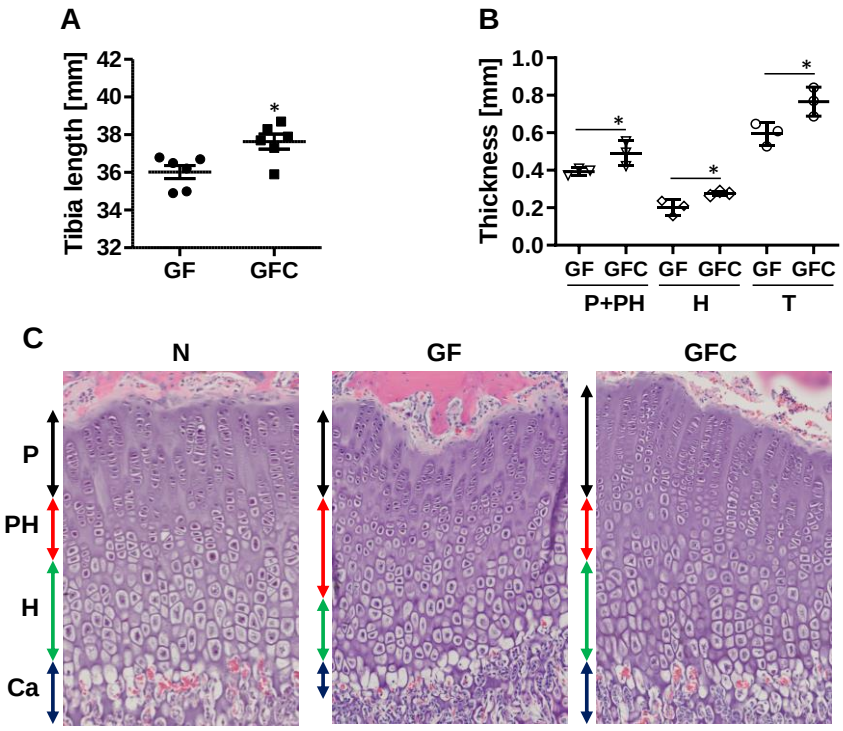

Figure 3. Microbiota-induced growth plate enlargement and improved chondrocyte maturation and calcification promote longitudinal bone growth. A. Total tibia length. B. Measurements of proximal tibia growth plate: P+PH - combined proliferative and prehypertrophic zone thickness (open triangles), H - hypertrophic zone thickness (open diamonds), and T – total thickness (open circles). C. Images of histologic specimens of normal (N), GF, and GFC growth plates. Two-headed arrows indicate growth plate zones, P - proliferative (black), PH - prehypertrophic (red), H - hypertrophic (green), and Ca – calcification (blue). *: $p<0.05$

epiphyseal plate in proximal tibia (Fig. 3). Mean tibial length was significantly increased by 1.6 mm in GFC rats over 10 day of conventionalization period with individual lengths ranging from 35.9 mm to 38.7 mm, while in GF rats the length range was from 34.9 mm to 36.8 mm (Fig. 3A). Reported longitudinal growth rate in Sprague-Dawley rats at 10 weeks of age is 97 $\pm$ 7 µm per day (Hansson et al., 1972). This comparison shows that tibia longitudinal growth rate was greatly accelerated in GFC rats which were gaining 160 µm of length per day over apparently lower growth rate in GF rats. Histologic examinations of decalcified sections of proximal tibia revealed that mean epiphyseal plate thickness was significantly increased in GFC animals by 29% and correlated with dramatic changes in morphology of the plate growth zones (Fig. 3B and 3C). Cumulative thickness of the proliferation and prehypertrophic zones in GFC animals was increased by 25%, while hypertrophic zone thickness was increased by 37%, as compared to GF animals (Fig. 3B). Changes in the thickness of growth plate zones were accompanied by substantial changes in their morphology (Fig. 3C). In GF rats as compared to normal rats, the proliferative and prehypertrophic zones, which deliver maturing chondrocytes, are characterized by low number of cells and affected spatial organization. Similarly, in hypertrophic zone, mature chondrocytes producing a matrix rich in collagen X are lower in number and are disorganized. These result in poorly developed calcification zone with affected vascular invasion, which is prerequisite for formation of primary spongiosa and trabecular bone in the process of endochondrial ossification. Remarkably, 10 days of exposure to host holobiont reversed all abnormalities of growth plate of GF rats, and reactivated proliferative zone which resulted in high number of dividing chondroblasts of discoidal shape and organized in characteristic regular columns (Fig. 3C). Thus, gut microbiome is directly involved in the regulation of longitudinal bone growth by acting on chondrocyte progression and maturation in GFC rats.

Reconstitution of gut microbiota increases bone marrow adiposity

Bone marrow adipose tissue (BMAT) is an essential component of the marrow environment contributing to hematopoeisis, osteogenesis and energy metabolism, and it responds to changes in diet, age, and energy demands (Horowitz et al., 2017; Li et al., 2019). BMAT constitutes of adipocytes with different functions depending on their origin and skeletal localization (Lecka-Czernik et al., 2017). In humans, in the so called “red marrow” where hematopoiesis occurs, adipocytes are dispersed among hematopoietic components and constitute 45% of cells. In contrast, the so called “yellow marrow” is composed of densely packed adipocytes constituting 95% of cells and is not permissive for hematopoiesis (Lecka-Czernik et al., 2017; Moore & Dawson, 1990). In mice, these two compartments are corresponding to BMAT located in proximal and distal tibia, respectively. Thus, in proximal tibia marrow adipocytes are dispersed and respond to environmental changes, such as cold exposure and caloric restriction, which prompted naming this depot as regulated marrow adipose tissue (rMAT). In contrast, BMAT located in the distal part of tibia consists of densely packed adipocytes and appears to be resistant to the environmental cues, prompting the name of constitutive marrow adipose tissue (cMAT) (Scheller et al., 2015). In rat tibia, rMAT is extending from the proximal location through the diaphysis past tibiofibular junction and is composed of small cells dispersed in marrow hematopoietic compartment, while cMAT is found in the distal tibia where cells are larger and densely packed. Little is known on the effect of microbiota on the BMAT function and the way the holobiont is involved in differentiation and regulation of the marrow adipocytes. We found that reconstitution of the holobiont in GFC rats increased adipocyte number and altered cell size distribution, as compared to GF animals (Fig. 4). Histologic evaluation of longitudinal sections of tibia diaphysis revealed increased adipocyte density by 26% and increased total area occupied

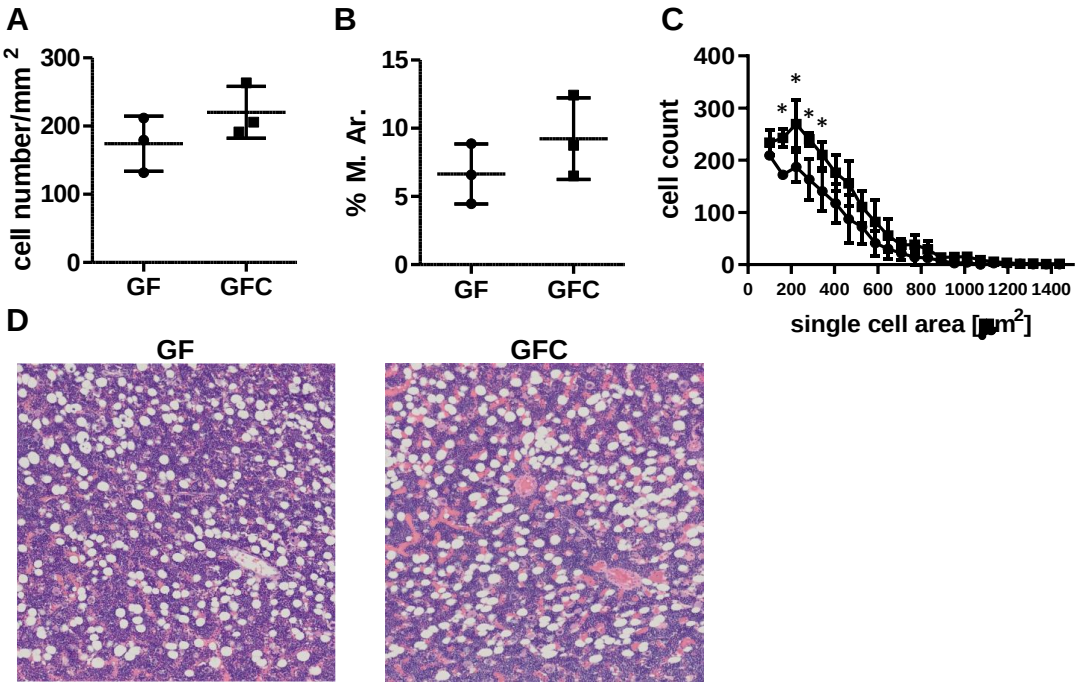

Figure 4. Effect of microbiota on bone marrow adiposity and size distribution of adipocytes. A. Mean adipocyte cell number per square millimeter of bone marrow. B. Percentage of marrow area (M.Ar) occupied by adipocytes in 12 mm long section of diaphysis. C. Quantitative distribution of adipocyte size in GF (black circles) and GFC (black squares) animals. D. Representative sections of bone marrow histologic specimens from GF and GFC rats. *: $p<0.05$

by adipocytes by 39% in GFC rats (Fig. 4A and 4B). These differences, although substantial, were not statistically significant. However, more detailed analysis of adipocyte size distribution (Fig. 4C) revealed that the number of smallest cells, ranging from 15 to 24 microns in diameter and constituting approximately 50% of all adipocytes present in the examined specimens, was nearly doubled in bone marrow of GFC rats while maintaining histology of adipocytes dispersed in marrow (Fig. 4D). Simultaneously, bone mass was significantly increased in GFC rats suggesting that *de novo* expansion of small size adipocytes and parallel osteoblast differentiation may result from microbiota-derived stimulus which promote general differentiation of MSC but not by redirecting differentiation of osteoblast/adipocyte common progenitor cells towards adipocytes (Lecka-Czernik et al., 1999).

Lack of evidence for genes which are directly involved in bone formation and resorption as underlying contributors to bone growth facilitated by microbiota

Next, we sought to identify putative effector genes responsible for the observed acceleration of bone mass accumulation in GFC rats by the analysis of gene expression using RNA isolated from bone marrow and bone tissue from tibia diaphysis. Collagen 1a1 (*Col1A1*), osteocalcin (*Bglap*), osterix (*Osx*) and sclerostin (*Sost*) were reporters of osteoblast/osteocyte activities and bone formation, whereas osteoprotegerin (*Opg*) and receptor activator of nuclear factor kappa-B ligand (*Rankl*) were reporters of the extent of osteoclastogenesis. Similarly, distal-less homeobox5 (*Dlx5*) and Wnt family member 10B (*Wnt10B*) were selected as markers of osteoblastogenesis, whereas Wnt family member 16 (*Wnt16*) and periostin (*Postn*) were used as markers of periosteal bone apposition. We also measured expression of adiponectin (*Adipoq*), fatty acid binding protein 4 (*Fabp4*) and peroxisome proliferator-activated receptor gamma (*Pparγ*) to assess bone-related activities of bone marrow adipocytes. Surprisingly, we did not detect any statistically significant differences in the expression of the analyzed genes neither in mineralized bone compartment nor in bone marrow, which were either expressed similarly in GF and GFC animals, or which expressions varied significantly within these groups (Supplementary Fig. 1 and Fig. 2). At this point we hypothesized that genes which are directly involved in bone formation and resorption, are less likely to be direct acceptors of regulatory signals resulting from bacterial colonization of the gut, leading us to shift our focus onto systemic regulatory factors.

Microbiota promote bone growth of the host *via* the short chain fatty acid butyrate as a metabolite signaling for IGF-1 expression

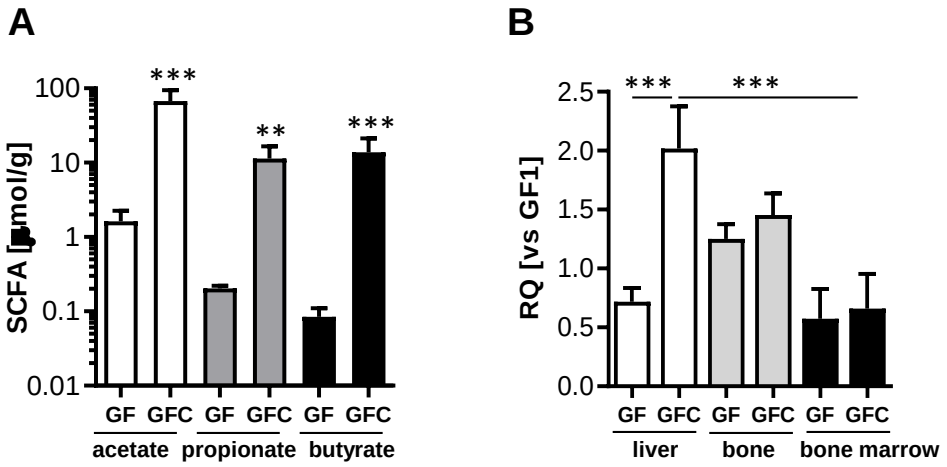

Figure 5. The effect of microbiota on cecal concentration of SCFA and concomitant *Igf-1* mRNA expression in liver, bone, and bone marrow. A. Cecal concentrations of acetate (white bars), propionate (grey bars), and butyrate (black bars) in GF and GFC rats. B. Relative quantities (RQ) of *Igf-1* transcripts measured by qPCR in liver (white bars), bone (grey bars), and bone marrow (black bars), relative to the highest value in GF group (GF1 rat). **: $p<0.01$, ***: $p<0.001$

To determine whether any of the microbial-generated metabolites in systemic circulation of the host were different between GF and GFC rats, we conducted a targeted metabolomics analysis of their ceca. All three short-chain fatty acids (SCFAs), acetate, propionate and butyrate were significantly higher in the GFC compared to GF rats (Fig. 5A). Importantly, a dramatic 160-fold increase was observed in the concentration of butyrate in GFC animals compared to GF rats. Butyrate is a known metabolite capable of signaling to regulate the IGF-1 anabolic effect on bone (S. Yakar et al., 2002; Yan et al., 2016). *Igf-1* is primarily expressed in liver and its availability is controlled by growth hormone (GH) and IGF-binding proteins (Pacifici, 2018; Silva et al., 2020). It is also locally expressed in bone cells and marrow mesenchymal stem cells (Lazarenko et al., 2007; Sheng et al., 2013)The level of *Igf-1* expression was significantly increased by 3-fold in the liver of GFC rats, whereas in GFC bone and bone marrow expression remained on the same level as in GF rats (Fig. 5B). Interestingly, GF animals are not devoid of *Igf-1* and do express this hormone, and GFC animals experienced significant but moderate *Igf-1*

upregulation. This observation suggests that reconstitution of microbiota results in *de novo* supply of butyrate which signals *via* modulation of *Igf-1* expression in the liver to restore the threshold of the circulating hormone to the level required for efficient bone formation (S. Yakar et al., 2002).

Elevated levels of serum markers of bone mineralization and liver function in GFC rats

To further explore systemic features aligned with the osteogenic effect resulting from the presence of newly established microbiota in GFC rats, we analyzed 15 blood serum markers and electrolytes indicative of bone, liver and kidney function (Table 1). Most of the assessed markers remained at comparable levels in GF and GFC animals, and were considered normal when compared to reference values published for normal wild-type male Sprague-Dawley rats (Col et al., 2009; Lillie et al., 1996; Zaias et al., 2009). These included protein and electrolyte markers, namely amylase (AMY), creatinine (CRE), globulin (GLOB), total protein (TP), phosphorous (Phos), sodium (Na) and potassium (K) (Table 1).

Table 1. Serum comprehensive diagnostic profile

Animal	ALB (g/dl)	ALP (U/L)	ALT (U/L)	AMY (U/L)	TBIL (mg/dl)	BUN (mg/dl)	Ca mg/dl	Phos (mg/dl)	CRE (mg/dl)	GLU (mg/dl)	Na (mmol/l)	K (mmol/l)	TP (g/dl)	GLOB (g/dl)
GF1	5.30	308.0	34.0	903.0	0.30	20.0	10.9	8.40	0.70	204.0	147.0	5.30	6.40	1.20
GF2	5.20	331.0	47.0	825.0	0.30	20.0	11.3	9.30	0.60	193.0	145.0	5.30	6.20	1.00
GF3	5.10	265.0	51.0	806.0	0.30	15.0	11.3	8.90	0.40	232.0	149.0	5.20	6.10	1.10
GF5	5.60	288.0	44.0	579.0	0.30	25.0	10.8	8.40	0.30	319.0	143.0	4.60	6.10	0.50
GF6	5.60	350.0	62.0	618.0	0.30	24.0	11.3	8.90	0.30	204.0	148.0	5.30	6.30	0.60
Mean	**5.36**	**308.4**	**47.6**	**746.2**	**0.30**	**20.8**	**11.1**	**8.78**	**0.46**	**230.4**	**146.4**	**5.14**	**6.22**	**0.88**
GFC1	5.00	415.0	37.0	831.0	0.30	19.0	10.9	9.80	0.20	241.0	144.0	5.10	5.80	0.90
GFC2	4.80	356.0	57.0	757.0	0.30	16.0	10.6	8.80	0.40	242.0	144.0	4.70	5.50	0.80
GFC3	4.40	343.0	84.0	790.0	0.30	18.0	10.2	9.30	0.20	231.0	143.0	5.30	5.30	0.90
GFC4	4.40	489.0	64.0	760.0	0.30	17.0	10.0	8.10	0.50	203.0	141.0	4.90	5.20	0.80
GFC5	4.40	460.0	39.0	720.0	0.30	19.0	10.4	8.30	0.60	220.0	143.0	5.20	5.20	0.90
GFC6	4.40	405.0	44.0	712.0	0.30	19.0	10.8	9.40	0.30	238.0	148.0	5.30	5.30	0.90
Mean	**4.57**	**411.3**	**54.2**	**761.7**	**0.30**	**18.0**	**10.5**	**8.95**	**0.37**	**229.2**	**143.8**	**5.08**	**5.38**	**0.87**
T-test	**0.001**	**0.006**	**0.490**	**0.803**	**1.000**	**0.134**	**0.008**	**0.627**	**0.392**	**0.956**	**0.106**	**0.738**	**0.0001**	**0.919**

[a)] Reference values were obtained from published sources cited in Materials and Methods section.

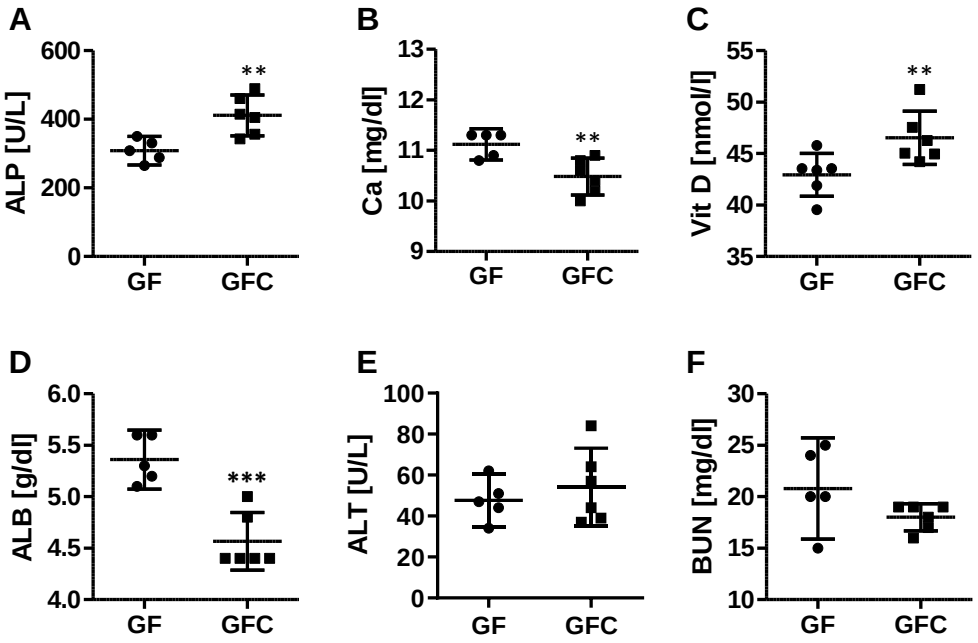

Figure 6. Changes in serum markers of bone mineralization and liver function in GF and GFC rats. Graphs A, B, and C respectively show bone markers concentrations of alkaline phosphatase (ALP), calcium (Ca), and vitamin D. Graphs D, E, and F show liver markers concentrations of albumin (ALB), alanine transaminase (ALT), and blood urea nitrogen (BUN). **: $p<0.01$, ***: $p<0.001$

In contrast, alkaline phosphatase (ALP) level was significantly elevated by 33% concurring *de novo* osteogenesis in GFC animals (Fig. 6A). Serum calcium concentration (Ca) was significantly decreased by 6% in GFC versus GF rats most likely as a result of increased bone formation (Fig. 6B), with 25-OH vitamin D serum level significantly increased by 8% (Fig. 6C) suggesting a physiologic response to increased calcium demand. Among the most prominent features was serum albumin (ALB), which was elevated in GF animals by 75%, as compared to reference values, and was significantly reduced in GFC rats to being elevated by only 48% (Fig. 6D). There is very limited information regarding hyperalbuminemia in animals and humans except that it is a rare condition which is mainly associated with dehydration (Walker et al., 1990). However, globulin level, albeit markedly lower than the reference value, was identical in

both groups with the total serum protein decrease following that of the albumin (Table 1), which indicated that dehydration was unlikely to be responsible for high albumin level.

Few veterinary cases were reported where hyperalbuminemia was associated with hepatocellular carcinoma, and a couple of cases in humans that were associated with prolonged ingestion of high protein diet (Cooper et al., 2009; Mutlu et al., 2006). Alanine transaminase (ALT), a marker of liver dysfunction, and blood urea nitrogen (BUN), a marker of kidney failure and increased protein degradation in liver, were evenly elevated but not different in both GF and GFC rats (Fig. 6E-F) by 75% and 52%, as compared to reference values shown in Table 1. However, creatinine readings were standard in both groups of animals suggesting normal kidney function. These observations imply that liver function, manifested by an increase in ALT and BUN, and unexpected elevation in ALB synthesis, is affected by the lack of microbiota and is not fully restored by a short-term presence of gut microbiota, except for partial normalization of ALB level.

Discussion

Recent advances in research addressing systemic gut host-microbiota interactions show that bone is a significant component of the holobiome being strongly tied to the status of gut microbiota. In this paper we show for the first time that *de novo* introduction of gut microbiota to GF rat can lead to abrupt increase in bone mass, acceleration of longitudinal bone growth and increased bone mineralization. To our knowledge, the observed phenotype is unprecedented considering that the observed changes occurred within 10-day time window following gut colonization. Further, one of the underlying mechanisms for the pronounced increase in bone growth was

traceable as mediated by the acute effects of signaling of the microbial metabolite, butyrate, to increase host *Igf-1*.

IGF-1 is crucial for normal growth and development of the skeleton and has been recognized as a hormone regulating cortical bone mass by acting on osteoblasts, and in combination with mechanical loading, increasing periosteal bone apposition (Gross et al., 2002) and longitudinal bone growth by augmenting hypertrophy of growth plate chondrocytes (Repudi et al., 2013; J. Wang et al., 1999). This is especially important in the context of skeletal development and maturation during adolescence, wherein production of IGF-1 is induced by circulating growth hormone. Our work here indicates that *Igf-1* is also regulated by acute exposure of the host to microbiota. Dramatic increase of cecal butyrate concentration observed in GFC rats paralleled with enhanced expression of *Igf-1* in the liver suggests that the somatotropic axis is one of the targets involved in bone enhancement. Recently, it has been shown that butyrate increases intracellular calcium levels and boost release of GH from pituitary acting on G-protein coupled receptors (Miletta et al., 2014). Although it was demonstrated that butyrate stimulates bone formation by increasing *Wnt10B* expression in bone marrow $CD8^+$ T cells (Tyagi et al., 2018), we did not detect any difference in the expression of this ligand in bone marrow of GF and GFC animals making WNT signaling pathway less likely to be involved. Significant increase in the expression level of liver *Igf-1* observed in GFC rats may also have resulted from a direct effect of butyrate signaling. It has been shown that consequent to gut microbiota-mediated increase in SCFA, the level of liver *Igf-1* is induced independently of GH stimulation and promotes bone formation (Yan et al., 2016). Parallel to endocrine action of circulating IGF-1 autocrine/paracrine signaling is achieved by its expression in all bone cell lineages and skeletal stem cells and exerting its effects on osteoblasts, osteocytes, and osteoclasts *via* IGF-1 receptor (Guntur &

Rosen, 2013; Y. Wang et al., 2013). The *Igf-1* mRNA expression in bone marrow and in bone tissue of GF and GFC rats were on the same level suggesting that the endocrine action of liver IGF-1 likely contributed to the accelerated bone formation in GFC animals.

Fermentation of complex carbohydrates in the colon by microbiota results in production SCFAs, acetate, propionate and butyrate, which act as regulatory metabolites on a variety of physiologic processes. Among them butyrate is a prominent modulator of bone homeostasis by affecting process of bone remodeling. Increased SCFA concentrations reduce osteoclastogenesis by shifting preosteoclast cellular metabolism towards glycolysis, block differentiation by inhibiting histone deacetylase, and in consequence limit bone resorption resulting in net gain of bone mass (Lucas et al., 2018; Rahman et al., 2003). On the other hand, butyrate upregulates osteoblast differentiation and proliferation by upregulation of WNT10b in bone marrow stromal cells resulting in increased bone formation (Tyagi et al., 2018). We postulate that in our model, SCFA, and particularly butyrate, is the primary signal which *in vivo* initiates cascade of molecular events leading to the acceleration of bone accrual.

Skeletal changes in GFC rats assessed in tibia bone were manifested by increased midshaft cortical thickness, expansion of trabecular bone, lengthening of tibia, and overall increase in bone size. All of these changes can be attributed to endocrine activity of circulating IGF-1. Analysis of cortical bone accrual revealed that bone gain in GFC animals was localized to the periosteal surface and formation of circumferential lamellar bone with no change to the endosteum, which is consistent with the overall endocrine effect of IGF-1 (Lindsey & Mohan, 2016; Stratikopoulos et al., 2008; Yakar et al., 2009). On the other hand, micro CT analysis of local changes in cortical bone thickness along tibia diaphysis showed that the maximal increase was localized to the anteromedial surface of tibia midshaft region, which is normally exposed to

maximal dynamic strain during habitual loading. It is accepted that anabolic effect of mechanical loading on the adaptative bone formation is tied to paracrine effect of locally expressed IGF-1 (Gross et al., 2002). Thus, the observed radial expansion of cortical bone in GFC animals most likely resulted from a combination of endocrine and paracrine effects of IGF-1 responding to the SCFA signal emerging from the reconstituted gut microbiota.

Reconstitution of gut microbiota in GFC animals had profound effect on the maturation of chondrocytes in the growth plate of proximal tibia and manifested by expansion of proliferative and hypertrophic zones and overall thickening of the epiphysis. This in turn accelerated longitudinal growth as compared to GF animals, as differentiation of proliferating chondrocytes into hypertrophic chondrocytes is crucial for bone lengthening (Tahimic et al., 2013). Again, maturation of epiphyseal chondrocytes remains under the control of IGF-1, similarly to the rest of bone forming cells (Reinecke et al., 2000). The observed phenomenon can be attributed to increased GH release from pituitary mediated by SCFA production in the gut, but it remains to be defined if paracrine, endocrine or both activities of IGF-1 are involved in this particular physiologic response.

Cortical thickness and the ratio of bone area to total cross-sectional area at tibia midshaft (B.Ar/T.Ar) in individual GF rats was positively correlated with their respective body mass, indicating that a fundamental principle of bone functional adaptation to body mass (Frost, 1987; Iwaniec & Turner, 2016) is maintained even in the absence of gut microbiota. However, we determined that these correlations are negative in GFC animals regardless of significant increase in their body weight, as compared to GF rats. This indicates that processes regulating bone accrual become temporarily independent of the mechanostat (Frost, 1987, 1996, 2003) and that additional mechanism(s) take over to accelerate bone growth and restore a balance between body

359 weight and skeleton resembling spurt growth naturally occurring in rats and humans
360 (Hermanussen et al., 1998; Roach et al., 2003; Styne, 2003).

361 Expansion of BMAT observed in GFC animals is an intriguing phenomenon because it was
362 accompanied by bone accumulation. However, bone accumulation in GFC rats occurs on the
363 periosteal surface thus reciprocal relationship between adipocytes and osteoblasts differentiation
364 from the common mesenchymal progenitor, which conforms belief that "marrow fat gain is bone
365 loss", seems to be not relevant in this model (Lecka-Czernik & Stechschulte, 2014; Z. Li et al.,
366 2018). On the other hand, BMAT is characterized with high heterogeneity reflecting both,
367 diverse origin of marrow adipocytes and different responsiveness to environmental cues. For
368 example, GH and IGF-1 axes, which are probably upregulated in our model, in general have a
369 negative effect on marrow adiposity making them less likely to be involved in observed BMAT
370 expansion (Menagh et al., 2010). Although very little is known about the effect of microbiota
371 and SCFA on marrow adipocytes, there are some indications of direct gut-BMAT
372 communication with one report showing spontaneous adipocytic differentiation of mesenchymal
373 cells derived from pig bone marrow in response to butyrate treatment (Tugnoli et al., 2019) and
374 the other showing increased adipogenesis and decreased osteogenesis in germ-free-
375 conventionalized mice (Xiao et al., 2017). However, besides determining axes stimulating
376 BMAT expansion in GFC rats, it is even more important to characterize the function of these
377 newly formed adipocytes. Several studies showed a spatial and functional correlation between
378 BMAT and active hematopoiesis suggesting that it is an important component of marrow niche
379 supporting hematopoiesis. It has been recognized that proliferation and differentiation of
380 myelopoietic cells in long term bone marrow cultures is supported by marrow adipocytes that
381 provide necessary cytokines, among them IL6, and perhaps energy in the form of heat and fuel

(Gimble et al., 2006) (Robles et al., 2019) and several recent studies have linked marrow adipocyte support for hematopoiesis with production of stroma differentiation factor (SDF) (Naveiras et al., 2009; Zhou et al., 2017). These, together with our circumstantial evidence of BMAT expansion after reconstitution of gut microbiome, provide preliminary clues on signaling axes and BMAT function in the context of holobiont, which need to be explored further.

The molecular mechanism that we have traced to the butyrate-mediated GH/Igf1 signaling pathway is recognized, however, it is significant to note that by virtue of employing the deconstruction of the holobiont in GF rats and reconstruction of the holobiont in GFC rats, our work here has provided a critical insight into the rapid nature of the physiologic interaction between bone and microbiota which leads to rapid bone accrual. Thus, our work defines microbiota as a factor to consider in targeting adolescent bone disorders and clinical management of age-related bone loss.

Materials and Methods

Animals

All animal experiments were conducted according to the University of Toledo Institutional Animal Care and Use Committee approved protocols. This study was conducted using male, 7-week-old Sprague Dawley (SD) rats that were concomitantly raised as gnotobiotic rats until the commencement of the study. Gnotobiotic rats were separated into two groups, either germ-free (GF) (n=6/group) or germ-free conventionalized (GFC) (n=6/group). These animals were raised and set up for studies at Taconic Biosciences (https://www.taconic.com/). Conventionalization of GFC rats were performed by co-housing GF rats with conventionally-raised SD rats for 10 days (1:1 ratio). Upon arrival at the University of Toledo, the animals were immediately used for

experiments. The animals were overdosed with isoflurane anesthesia and blood and tissue were collected and stored for further use.

Collection and processing of specimens

Femurs and tibias extracted from sacrificed animals were thoroughly cleaned of muscle tissue. Both tibias from each animal were immediately preserved in 10% NBF for subsequent evaluation of bone microstructure and for preparation of histological sections. For RNA isolations from bone and marrow single femur was kept on ice after extraction and processed as follows. Proximal and distal ends were cut off using rotary diamond micro saw, diaphysis bone sections were suspended in a hole drilled in microtube lid, and then bone and marrow were separated by centrifugation at 2000 x g for 1 min at 4^{o}C. Following separation bone and marrow were flash frozen in liquid nitrogen. Tibias intended for preparation of histological sections were kept in 10% NBF for 3 days, then decalcified on a rocking platform with Formical-4 reagent (StatLab, McKinney, TX, USA) in 3 consecutive extractions lasting 24, 6, and 2 hours using 20 ml of the decalcifier. Oxalic acid test was conducted on the last fraction to ensure the complete calcium removal and decalcified bones were stored in 10% NBF for further processing. Cecal SCFAs were analyzed as described (Singh et al., 2018).

Bone morphometry

Assessment of trabecular bone in proximal tibia and cortical bone at tibia midshaft was conducted by micro CT using µCT 35 system (Scanco Medical AG, Bruettisellen, Switzerland). Bone scans were performed with the x-ray source operating at 70 kVp and 114 µA energy settings, and recording 500 projections/180^{o} acquired at 300 ms integration time using 20 µm nominal resolution voxel for both bone locations. Scans of the proximal tibia consisted of 340

cross-sectional slices starting at the top of growth plate, and images of trabecular bone were segmented at optimized lower threshold value of 220 using per mille scale (approximately 3000 HU, or μ of 1.76) following manual contouring starting 10 slices down from the intercondylar notch and extending for 200 more slices. Scans of the cortical bone at tibia midshaft contained 57 slices all of which were contoured automatically, and which were segmented at 260 per mille threshold. Computed bone bending strength (I_{max}/C_{max} and I_{min}/C_{min}) and torsional strength (pMOI) at tibia midshaft were based on bone cross-sectional geometry in combination with local tissue mineral content. The analysis of the trabecular bone microstructure, cortical bone parameters, and bone strength, was conducted using Evaluation Program V6.5-3 (Scanco Medical AG) and conformed to recommended guidelines (Bouxsein et al., 2010)

Gene expression

Total RNAs from bone tissue and marrow specimens were isolated using TRI Reagent (MRC Inc., Cincinnati, OH, USA) following manufacturers' protocol. Frozen marrow and bone were directly homogenized in TRI Reagent using microtube pistons and rotor-stator homogenizer, respectively. cDNAs were synthesized using 0.25 μg of isolated RNAs and Verso cDNA Synthesis Kit (Thermo Fisher Scientific, Waltham, MA, USA). Oligonucleotide primers for real-time qPCR were designed using Primer-Blast (NCBI, NIH) with PCR product length set from 80 to 120 nucleotides and 60^{o} C optimal primer melting temperature. Oligonucleotides were synthesized by the Integrated DNA Technologies, Inc. (Coralville, IA, USA) and melting temperatures, adjusted for qPCR conditions, were calculated using OligoAnalyzer Tool available at the manufacturer's website. Oligonucleotide sequences, amplicon sizes, and melting temperatures are listed in the Supplementary Table 1. qPCR amplifications were carried out using TruAmp qPCR SYBR Green SuperMix-Rox (Smart Bioscience Inc., Maumee, OH, USA)

and StepOne Plus system (Applied Biosystems Inc., Foster City, CA, USA). Amplifications were carried out using 40 cycle two-step amplification protocol with annealing temperatures set to 4-5 degrees below calculated primers melting temperatures, and finished with melting curve cycle to verify homogeneity of amplification products. Relative gene expression was analyzed by the comparative ΔΔCT method using *18S* RNA levels for normalization.

Histology and image quantification

Decalcified femur bones were segmented at tibia crest and tibiofibular junction, and resulting proximal and mid diaphysis fragments were embedded in paraffin blocks and processed at the University of Toledo Histology Core Facility. High resolution images of longitudinal 6 µm sections stained with H&E were generated using Olympus VS120 slide scanner. Images in the native VSI format were converted to TIFF images at the resolution of 0.685 µm/pixel which were then used for histological analysis. Image conversion and subsequent measurements of circumferential lamellar bone, growth plate, and marrow adiposity were conducted using tools available in Fiji-ImageJ image processing package (Schindelin et al., 2012) equipped with OlympusViewer Plugin (Olympus Corp., Tokyo, Japan). Determination of adipocyte count and cell size distribution in bone marrow was done on 8-bit grayscale images after applying grayscale threshold of 210-254 which effectively separated adipocytes from the majority of bone marrow cellular components (histogram peak). Since bone marrow adipocytes significantly differ in size, 3 random bone marrow 0.3 mm^2 areas were sampled and it was determined that histologically relevant single adipocyte area was within the range of 90-1400 μm^2. In order to eliminate irregular objects of similar areas roundness threshold was set to 0.4, which was equivalent to a 2.5 aspect ratio.

Serum chemistry

GF and GFC rats were euthanized by CO_2 asphyxiation and blood was collected *via* cardiac puncture during euthanasia in BD microtainer (Becton, Dickinson, Franklin Lakes, NJ). Hemolysis-free sera were obtained after centrifugation 10,000 rpm, 10 min, 4°C and stored at -80°C until further use. Automated assessment of serum markers was conducted using VetScan 2 analyzer (Abaxis, Inc., Union City, CA, USA) and Comprehensive Diagnostic Profile rotor (Abaxis 500-7123) which contains tests for alanine aminotransferase (ALT), albumin (ALB), alkaline phosphatase(ALP), amylase (AMY), total calcium (C++), creatinine (CRE), globulin (GLOB), glucose (GLU), phosphorus (PHOS), potassium (K+), sodium (Na+), total bilirubin (TBIL), total protein (TP), and blood urea nitrogen (BUN). Serum preparation and measurements were conducted according to a protocol provided by the manufacturer.

Statistical analysis

Data are presented as means $\pm$ SD. Statistical analysis was performed using two-tailed Student's test and Pearson correlation to compare animal groups using GraphPad Prism 8.3 (GraphPad, La Jolla, CA, USA). Statistical differences with $p < 0.05$ were considered significant.

Acknowledgements

This work was supported by grants from the NIH to BJ and MVK (HL1430820 and CA219144, respectively), American Diabetes Association Innovative Basic Science Award (1-19-IBS-029) to BLC, and grant from the Crohn's and Colitis foundation to PS (Ref.# 522820)

Authors' roles: BJ, BLC, MVK, PJC contributed to experimental design, data analysis, and data interpretation; BSY, MVK PJC, RMG, SC, PS, BM conducted the experiments, PJC wrote the manuscript, BJ, BLC, MVK and PJC edited the manuscript, and take responsibility for the integrity of the data analysis.

References

Bouxsein, M. L., Boyd, S. K., Christiansen, B. A., Guldberg, R. E., Jepsen, K. J., & Muller, R. (2010). Guidelines for assessment of bone microstructure in rodents using micro-computed tomography. *J Bone Miner Res, 25*(7), 1468-1486. doi:10.1002/jbmr.141

Britton, R. A., Irwin, R., Quach, D., Schaefer, L., Zhang, J., Lee, T., . . . McCabe, L. R. (2014). Probiotic L. reuteri treatment prevents bone loss in a menopausal ovariectomized mouse model. *J Cell Physiol, 229*(11), 1822-1830. doi:10.1002/jcp.24636

Col, C., Dinler, K., Hasdemir, A. O., & Bugdayci, G. (2009). The effect of an intraperitoneal injection of melatonin on serum amylase levels in acute pancreatitis. *Jop, 10*(3), 306-309.

Cooper, E. S., Wellman, M. L., & Carsillo, M. E. (2009). Hyperalbuminemia associated with hepatocellular carcinoma in a dog. *Vet Clin Pathol, 38*(4), 516-520. doi:10.1111/j.1939-165X.2009.00153.x

Davis, C. D. (2016). The Gut Microbiome and Its Role in Obesity. *Nutr Today, 51*(4), 167-174. doi:10.1097/nt.0000000000000167

Frost, H. M. (1987). Bone "mass" and the "mechanostat": a proposal. *Anat Rec, 219*(1), 1-9. doi:10.1002/ar.1092190104

Frost, H. M. (1996). Perspectives: a proposed general model of the "mechanostat" (suggestions from a new skeletal-biologic paradigm). *Anat Rec, 244*(2), 139-147. doi:10.1002/(sici)1097-0185(199602)244:2<139::aid-ar1>3.0.co;2-x

Frost, H. M. (2003). Bone's mechanostat: a 2003 update. *Anat Rec A Discov Mol Cell Evol Biol, 275*(2), 1081-1101. doi:10.1002/ar.a.10119

Gimble, J. M., Zvonic, S., Floyd, Z. E., Kassem, M., & Nuttall, M. E. (2006). Playing with bone and fat. *Journal of Cellular Biochemistry, 98*(2), 251-266. doi:10.1002/jcb.20777

Gross, T. S., Srinivasan, S., Liu, C. C., Clemens, T. L., & Bain, S. D. (2002). Noninvasive loading of the murine tibia: an in vivo model for the study of mechanotransduction. *J Bone Miner Res, 17*(3), 493-501. doi:10.1359/jbmr.2002.17.3.493

Guntur, A. R., & Rosen, C. J. (2013). IGF-1 regulation of key signaling pathways in bone. *Bonekey Rep, 2*, 437. doi:10.1038/bonekey.2013.171

Gurung, M., Li, Z., You, H., Rodrigues, R., Jump, D. B., Morgun, A., & Shulzhenko, N. (2020). Role of gut microbiota in type 2 diabetes pathophysiology. *EBioMedicine, 51*, 102590. doi:10.1016/j.ebiom.2019.11.051

Hansson, L. I., Menander-Sellman, K., Stenstrom, A., & Thorngren, K. G. (1972). Rate of normal longitudinal bone growth in the rat. *Calcif Tissue Res, 10*(3), 238-251. doi:10.1007/bf02012553

Hermanussen, M., Rol de Lama, M. A., JA, F. T., Grasedyck, L., & Burmeister, J. (1998). Short-term growth: evidence for chaotic series of mini growth spurts in rat growth. *Physiol Behav, 64*(1), 7-13. doi:10.1016/s0031-9384(98)00023-7

Hernandez, C. J., Guss, J. D., Luna, M., & Goldring, S. R. (2016). Links Between the Microbiome and Bone. *J Bone Miner Res, 31*(9), 1638-1646. doi:10.1002/jbmr.2887

Horowitz, M. C., Berry, R., Holtrup, B., Sebo, Z., Nelson, T., Fretz, J. A., . . . Rosen, C. J. (2017). Bone marrow adipocytes. *Adipocyte, 6*(3), 193-204. doi:10.1080/21623945.2017.1367881

Iwaniec, U. T., & Turner, R. T. (2016). Influence of body weight on bone mass, architecture and turnover. *J Endocrinol, 230*(3), R115-130. doi:10.1530/joe-16-0089

Kang, B. H., Kim, S. H., Jung, K. A., Kim, S. Y., Chung, S. H., Park, Y. S., . . . Shim, K. S. (2015). Comparison of growth and pubertal progression in wild type female rats with different bedding types. *Ann Pediatr Endocrinol Metab, 20*(1), 53-58. doi:10.6065/apem.2015.20.1.53

Lazarenko, O. P., Rzonca, S. O., Hogue, W. R., Swain, F. L., Suva, L. J., & Lecka-Czernik, B. (2007). Rosiglitazone induces decreases in bone mass and strength that are reminiscent of aged bone. *Endocrinology, 148*(6), 2669-2680. doi:10.1210/en.2006-1587

Lecka-Czernik, B., Gubrij, I., Moerman, E. J., Kajkenova, O., Lipschitz, D. A., Manolagas, S. C., & Jilka, R. L. (1999). Inhibition of Osf2/Cbfa1 expression and terminal osteoblast differentiation by PPARgamma2. *J Cell Biochem, 74*(3), 357-371.

Lecka-Czernik, B., & Stechschulte, L. A. (2014). Bone and fat: A relationship of different shades. *Archives of Biochemistry and Biophysics, 561*, 124-129. doi:https://doi.org/10.1016/j.abb.2014.06.010

Lecka-Czernik, B., Stechschulte, L. A., Czernik, P. J., Sherman, S. B., Huang, S., & Krings, A. (2017). Marrow Adipose Tissue: Skeletal Location, Sexual Dimorphism, and Response to

555 Sex Steroid Deficiency. *Frontiers in Endocrinology, 8*(188).
556 doi:10.3389/fendo.2017.00188
557 Li, J. Y., Chassaing, B., Tyagi, A. M., Vaccaro, C., Luo, T., Adams, J., . . . Pacifici, R. (2016).
558 Sex steroid deficiency-associated bone loss is microbiota dependent and prevented by
559 probiotics. *J Clin Invest, 126*(6), 2049-2063. doi:10.1172/jci86062
560 Li, Y., Meng, Y., & Yu, X. (2019). The Unique Metabolic Characteristics of Bone Marrow
561 Adipose Tissue. *Front Endocrinol (Lausanne), 10*, 69. doi:10.3389/fendo.2019.00069
562 Li, Z., Hardij, J., Bagchi, D. P., Scheller, E. L., & MacDougald, O. A. (2018). Development,
563 regulation, metabolism and function of bone marrow adipose tissues. *Bone, 110*, 134-140.
564 doi:10.1016/j.bone.2018.01.008
565 Lillie, L. E., Temple, N. J., & Florence, L. Z. (1996). Reference values for young normal
566 Sprague-Dawley rats: weight gain, hematology and clinical chemistry. *Hum Exp Toxicol,*
567 *15*(8), 612-616. doi:10.1177/096032719601500802
568 Lindsey, R. C., & Mohan, S. (2016). Skeletal effects of growth hormone and insulin-like growth
569 factor-I therapy. *Mol Cell Endocrinol, 432*, 44-55. doi:10.1016/j.mce.2015.09.017
570 Lucas, S., Omata, Y., Hofmann, J., Bottcher, M., Iljazovic, A., Sarter, K., . . . Zaiss, M. M.
571 (2018). Short-chain fatty acids regulate systemic bone mass and protect from pathological
572 bone loss. *Nat Commun, 9*(1), 55. doi:10.1038/s41467-017-02490-4
573 Margulis, L., & Fester, R. (1991). *Symbiosis as a source of evolutionary innovation : speciation*
574 *and morphogenesis*: Cambridge (Mass.) : MIT press.
575 Medicine, N. L. o. (2020). Clinical trials. Retrieved from https://clinicaltrials.gov/
576 Menagh, P. J., Turner, R. T., Jump, D. B., Wong, C. P., Lowry, M. B., Yakar, S., . . . Iwaniec, U.
577 T. (2010). Growth hormone regulates the balance between bone formation and bone
578 marrow adiposity. *J Bone Miner Res, 25*(4), 757-768. doi:10.1359/jbmr.091015
579 Miletta, M. C., Petkovic, V., Eble, A., Ammann, R. A., Fluck, C. E., & Mullis, P. E. (2014).
580 Butyrate increases intracellular calcium levels and enhances growth hormone release
581 from rat anterior pituitary cells via the G-protein-coupled receptors GPR41 and 43. *PLoS*
582 *One, 9*(10), e107388. doi:10.1371/journal.pone.0107388
583 Moore, S. G., & Dawson, K. L. (1990). Red and yellow marrow in the femur: age-related
584 changes in appearance at MR imaging. *Radiology, 175*(1), 219-223.
585 doi:10.1148/radiology.175.1.2315484

586 Mutlu, E. A., Keshavarzian, A., & Mutlu, G. M. (2006). Hyperalbuminemia and elevated
587 transaminases associated with high-protein diet. *Scand J Gastroenterol, 41*(6), 759-760.
588 doi:10.1080/00365520500442625
589 Naveiras, O., Nardi, V., Wenzel, P. L., Hauschka, P. V., Fahey, F., & Daley, G. Q. (2009). Bone-
590 marrow adipocytes as negative regulators of the haematopoietic microenvironment.
591 *Nature, 460*(7252), 259-263. doi:10.1038/nature08099
592 Pacifici, R. (2018). Bone Remodeling and the Microbiome. *Cold Spring Harb Perspect Med,*
593 *8*(4). doi:10.1101/cshperspect.a031203
594 Park, O. J., Kim, J., Yang, J., Yun, C. H., & Han, S. H. (2017). Muramyl Dipeptide, a Shared
595 Structural Motif of Peptidoglycans, Is a Novel Inducer of Bone Formation through
596 Induction of Runx2. *J Bone Miner Res, 32*(7), 1455-1468. doi:10.1002/jbmr.3137
597 Rahman, M. M., Kukita, A., Kukita, T., Shobuike, T., Nakamura, T., & Kohashi, O. (2003). Two
598 histone deacetylase inhibitors, trichostatin A and sodium butyrate, suppress
599 differentiation into osteoclasts but not into macrophages. *Blood, 101*(9), 3451-3459.
600 doi:10.1182/blood-2002-08-2622
601 Reinecke, M., Schmid, A. C., Heyberger-Meyer, B., Hunziker, E. B., & Zapf, J. (2000). Effect of
602 growth hormone and insulin-like growth factor I (IGF-I) on the expression of IGF-I
603 messenger ribonucleic acid and peptide in rat tibial growth plate and articular
604 chondrocytes in vivo. *Endocrinology, 141*(8), 2847-2853. doi:10.1210/endo.141.8.7624
605 Repudi, S. R., Patra, M., & Sen, M. (2013). WISP3-IGF1 interaction regulates chondrocyte
606 hypertrophy. *J Cell Sci, 126*(Pt 7), 1650-1658. doi:10.1242/jcs.119859
607 Roach, H. I., Mehta, G., Oreffo, R. O., Clarke, N. M., & Cooper, C. (2003). Temporal analysis of
608 rat growth plates: cessation of growth with age despite presence of a physis. *J Histochem*
609 *Cytochem, 51*(3), 373-383. doi:10.1177/002215540305100312
610 Robles, H., Park, S., Joens, M. S., Fitzpatrick, J. A. J., Craft, C. S., & Scheller, E. L. (2019).
611 Characterization of the bone marrow adipocyte niche with three-dimensional electron
612 microscopy. *Bone, 118*, 89-98. doi:10.1016/j.bone.2018.01.020
613 Scheller, E. L., Doucette, C. R., Learman, B. S., Cawthorn, W. P., Khandaker, S., Schell, B., . . .
614 MacDougald, O. A. (2015). Region-specific variation in the properties of skeletal
615 adipocytes reveals regulated and constitutive marrow adipose tissues. *Nature*
616 *Communications, 6*(1), 7808. doi:10.1038/ncomms8808

Schepper, J. D., Irwin, R., Kang, J., Dagenais, K., Lemon, T., Shinouskis, A., . . . McCabe, L. R. (2017). Probiotics in Gut-Bone Signaling. *Adv Exp Med Biol, 1033*, 225-247. doi:10.1007/978-3-319-66653-2_11

Schindelin, J., Arganda-Carreras, I., Frise, E., Kaynig, V., Longair, M., Pietzsch, T., . . . Cardona, A. (2012). Fiji: an open-source platform for biological-image analysis. *Nat Methods, 9*(7), 676-682. doi:10.1038/nmeth.2019

Sender, R., Fuchs, S., & Milo, R. (2016). Revised Estimates for the Number of Human and Bacteria Cells in the Body. *PLoS Biol, 14*(8), e1002533. doi:10.1371/journal.pbio.1002533

Sheng, M. H., Zhou, X. D., Bonewald, L. F., Baylink, D. J., & Lau, K. H. (2013). Disruption of the insulin-like growth factor-1 gene in osteocytes impairs developmental bone growth in mice. *Bone, 52*(1), 133-144. doi:10.1016/j.bone.2012.09.027

Silva, Y. P., Bernardi, A., & Frozza, R. L. (2020). The Role of Short-Chain Fatty Acids From Gut Microbiota in Gut-Brain Communication. *Front Endocrinol (Lausanne), 11*, 25. doi:10.3389/fendo.2020.00025

Simon, J.-C., Marchesi, J. R., Mougel, C., & Selosse, M.-A. (2019). Host-microbiota interactions: from holobiont theory to analysis. *Microbiome, 7*(1), 5. doi:10.1186/s40168-019-0619-4

Singh, V., Yeoh, B. S., Chassaing, B., Xiao, X., Saha, P., Aguilera Olvera, R., . . . Vijay-Kumar, M. (2018). Dysregulated Microbial Fermentation of Soluble Fiber Induces Cholestatic Liver Cancer. *Cell, 175*(3), 679-694.e622. doi:10.1016/j.cell.2018.09.004

Sjögren, K., Engdahl, C., Henning, P., Lerner, U. H., Tremaroli, V., Lagerquist, M. K., . . . Ohlsson, C. (2012). The gut microbiota regulates bone mass in mice. *J Bone Miner Res, 27*(6), 1357-1367. doi:10.1002/jbmr.1588

Stenstrom, A., Hansson, L. I., & Thorngren, K. G. (1977). Cortical bone remodeling in normal rat. *Calcif Tissue Res, 23*(2), 161-170. doi:10.1007/bf02012782

Stratikopoulos, E., Szabolcs, M., Dragatsis, I., Klinakis, A., & Efstratiadis, A. (2008). The hormonal action of IGF1 in postnatal mouse growth. *Proc Natl Acad Sci U S A, 105*(49), 19378-19383. doi:10.1073/pnas.0809223105

Styne, D. M. (2003). The Regulation of Pubertal Growth. *Hormone Research in Paediatrics, 60(suppl 1)*(Suppl. 1), 22-26. doi:10.1159/000071222

Tahimic, C. G., Wang, Y., & Bikle, D. D. (2013). Anabolic effects of IGF-1 signaling on the skeleton. *Front Endocrinol (Lausanne), 4*, 6. doi:10.3389/fendo.2013.00006

Tam, C. S., Harrison, J. E., Reed, R., & Cruickshank, B. (1978). Bone apposition rate as an index of bone metabolism. *Metabolism, 27*(2), 143-150. doi:10.1016/0026-0495(78)90160-9

Tugnoli, B., Bernardini, C., Forni, M., Piva, A., Stahl, C. H., & Grilli, E. (2019). Butyric acid induces spontaneous adipocytic differentiation of porcine bone marrow-derived mesenchymal stem cells. *In Vitro Cell Dev Biol Anim, 55*(1), 17-24. doi:10.1007/s11626-018-0307-x

Tyagi, A. M., Yu, M., Darby, T. M., Vaccaro, C., Li, J. Y., Owens, J. A., . . . Pacifici, R. (2018). The Microbial Metabolite Butyrate Stimulates Bone Formation via T Regulatory Cell-Mediated Regulation of WNT10B Expression. *Immunity, 49*(6), 1116-1131.e1117. doi:10.1016/j.immuni.2018.10.013

Walker, H. K., Hall, W. D., & Hurst, J. W. (1990). *Clinical methods : the history, physical, and laboratory examinations*. Boston: Butterworths.

Wang, J., Zhou, J., & Bondy, C. A. (1999). Igf1 promotes longitudinal bone growth by insulin-like actions augmenting chondrocyte hypertrophy. *Faseb j, 13*(14), 1985-1990. doi:10.1096/fasebj.13.14.1985

Wang, Y., Bikle, D. D., & Chang, W. (2013). Autocrine and Paracrine Actions of IGF-I Signaling in Skeletal Development. *Bone Res, 1*(3), 249-259. doi:10.4248/br201303003

Weingarden, A. R., & Vaughn, B. P. (2017). Intestinal microbiota, fecal microbiota transplantation, and inflammatory bowel disease. *Gut Microbes, 8*(3), 238-252. doi:10.1080/19490976.2017.1290757

Xiao, E., He, L., Wu, Q., Li, J., He, Y., Zhao, L., . . . Zhang, Y. (2017). Microbiota regulates bone marrow mesenchymal stem cell lineage differentiation and immunomodulation. *Stem Cell Res Ther, 8*(1), 213. doi:10.1186/s13287-017-0670-7

Xu, X., Jia, X., Mo, L., Liu, C., Zheng, L., Yuan, Q., & Zhou, X. (2017). Intestinal microbiota: a potential target for the treatment of postmenopausal osteoporosis. *Bone Res, 5*, 17046. doi:10.1038/boneres.2017.46

Yakar, S., Canalis, E., Sun, H., Mejia, W., Kawashima, Y., Nasser, P., . . . Rosen, C. (2009). Serum IGF-1 determines skeletal strength by regulating subperiosteal expansion and trait

678 interactions. *Journal of Bone and Mineral Research, 24*, 1481-1492.
679 doi:10.1359/jbmr.090226
680 Yakar, S., Rosen, C. J., Beamer, W. G., Ackert-Bicknell, C. L., Wu, Y., Liu, J. L., . . . LeRoith,
681 D. (2002). Circulating levels of IGF-1 directly regulate bone growth and density. *J Clin*
682 *Invest, 110*(6), 771-781. doi:10.1172/jci15463
683 Yan, J., & Charles, J. F. (2017). Gut Microbiome and Bone: to Build, Destroy, or Both? *Curr*
684 *Osteoporos Rep, 15*(4), 376-384. doi:10.1007/s11914-017-0382-z
685 Yan, J., Herzog, J. W., Tsang, K., Brennan, C. A., Bower, M. A., Garrett, W. S., . . . Charles, J.
686 F. (2016). Gut microbiota induce IGF-1 and promote bone formation and growth. *Proc*
687 *Natl Acad Sci U S A, 113*(47), E7554-e7563. doi:10.1073/pnas.1607235113
688 Zaias, J., Mineau, M., Cray, C., Yoon, D., & Altman, N. H. (2009). Reference values for serum
689 proteins of common laboratory rodent strains. *J Am Assoc Lab Anim Sci, 48*(4), 387-390.
690 Zhou, B. O., Yu, H., Yue, R., Zhao, Z., Rios, J. J., Naveiras, O., & Morrison, S. J. (2017). Bone
691 marrow adipocytes promote the regeneration of stem cells and haematopoiesis by
692 secreting SCF. *Nat Cell Biol, 19*(8), 891-903. doi:10.1038/ncb3570

693